Available online at www.sciencedirect.com
ScienceDirect
Acta Materialia xxx (2010) xxx–xxx
Acta MATERIALIA
www.elsevier.com/locate/actamat

Permeability, pore connectivity and critical pore throat control of expandable polymeric sphere templated macroporous alumina

Linnéa Andersson [a,b], Anthony C. Jones [b], Mark A. Knackstedt [b], Lennart Bergström [a,*]

[a] Department of Materials and Environmental Chemistry, Stockholm University, SE-106 91 Stockholm, Sweden
[b] Department of Applied Mathematics, Research School of Physical Sciences and Engineering, Australian National University, Canberra ACT 0200, Australia

Received 8 July 2010; received in revised form 25 October 2010; accepted 26 October 2010

Abstract

We have regulated the permeability in macroporous alumina materials by manipulating the connectivity of the pore phase and the sizes of the smallest constrictions between connected pores. Templating with particle-coated expandable polymeric spheres (EPS) significantly increased the fraction of isolated pore clusters, and reduced both the sizes and the number of connections with neighboring pores, as determined by three-dimensional evaluation with X-ray micro-computed tomography. The stable particle coating, applied onto the EPS surfaces using polyelectrolyte multilayers, reduced the volume expansion and the coalescence of the EPS at elevated temperatures, which reduced the simulated permeability by as much as two orders of magnitude compared to templating with uncoated EPS in materials of similar porosities. We show that the Katz–Thompson model accurately predicts the permeability for the macroporous alumina materials with porosities of 46–76%. This suggests that the permeability to fluid flow in these materials is governed by the smallest constrictions between connected pores: the critical pore throat diameter.

Keywords: X-ray computed tomography; Permeability; Porous material; Alumina (α-Al_2O_3); Expandable polymeric spheres

1. Introduction

Macroporous ceramics with open pore structures are found in numerous applications ranging from catalyst supports [1,2], particulate filters for diesel engines [3,4], filtration of molten metal [5] and as biomedical scaffolds and implants [6,7]. Each application has specific requirements for the macroporous material with respect to properties such as pressure drop and permeability. These requirements are related to characteristics of the material such as the pore size and pore connectivity. Catalysis applications typically require a high degree of connected porosity and a hierarchical pore size distribution to achieve high permeability, high degree of access to the active surface area and a low pressure drop [1]. Filtration of molten metal requires ceramic foams of high strength with a well-defined pore size and permeability [4,5]. Porous ceramics in biomedical applications require a pore size distribution, porosity and pore connectivity optimized for integration with living tissue and, if necessary, load-bearing strength [6,7]. In contrast, thermal insulating panels for aerospace applications and kilns require ceramic materials with a high porosity but low connectivity to minimize convective heat transport [2,4].

The number of neighboring pores that are connected, and the size of the constrictions between these connected pores, i.e. the cell windows or pore throats, have a strong impact on the resistance to fluid flow through porous ceramics [5,8,9]. These parameters are not easily quantified with established methods like mercury porosimetry and scanning electron microscopy. Three-dimensional (3D) information from X-ray micro-computed tomography (μ-CT), however, can be used to determine the structural parameters, visualize the porous structure and also to simulate the permeability [10–13].

* Corresponding author. Tel.: +46 8 16 23 68; fax: +46 8 15 21 87.
E-mail address: lennart.bergstrom@mmk.su.se (L. Bergström).

1359-6454/$36.00 © 2010 Acta Materialia Inc. Published by Elsevier Ltd. All rights reserved.
doi:10.1016/j.actamat.2010.10.056

Macroporous ceramics can be produced by various methods that typically rely on the use of sacrificial templating materials or by direct foaming of the ceramic suspensions [4,14]. Industrial production of porous ceramics for filtration of molten metal and exhaust filters for diesel engines is based on the impregnation of a polymer foam with a concentrated ceramic suspension [2]. The polymer foam shapes the pores and is removed in a pyrolysis step before sintering. This is a simple and straightforward technique but it is difficult to produce materials with pore sizes smaller than 200 μm [14] or to alter the connectivity of the porous phase [14,15]. Another technique is to form macroporous ceramic materials from surfactant or particle stabilized foams or emulsions [14,16]. This technique can yield highly porous ceramic materials but usually renders materials with small pore throats [2,14,15]. The use of dense or hollow polymer beads as a sacrificial templating material offers significant versatility to control the porosity and pore size distribution [17,18]. It was recently demonstrated [19] how expandable polymeric spheres (EPS) can be used to produce highly porous materials with tunable pore size, using very low amounts of organic material in the cast powder bodies. A unique advantage of this technique is the temperature-induced expansion of the EPS and the associated volume increase of the suspension that can be used as a near-net shaping method. However, the control of the connectivity of the porous phase with the original technique is limited.

In this study, we show how the connectivity and the size of the pore throats can be controlled by coating the surfaces of the expandable spheres using a polyelectrolyte-based layer-by-layer process. The surface modification process and the dense particle coating on the EPS were characterized by electrokinetic mobility measurements, scanning electron microscopy and thermogravimetry. After casting and template removal, the macroporous materials were characterized with a combination of X-ray μ-CT, mercury porosimetry and scanning electron microscopy. These techniques yielded information on the total porosity, pore size distribution, pore throat size distribution and pore connectivity. The permeability to fluid flow was simulated on 3D datasets retrieved with X-ray μ-CT and compared to predictions based on the Katz–Thompson model [20]. We found that sacrificial templating with particle-coated and non-coated EPS could be used to control three critical parameters of the porous phase that determine the permeability to fluid flow: the fraction of pores connected into a percolating pore phase, the critical pore throat diameter and the number of connections with neighboring pores.

2. Methods and materials

2.1. Materials and procedures

The procedure to produce the macroporous alumina is schematically described in Fig. 1. We used expandable polymeric spheres (EPS) as a templating agent to shape

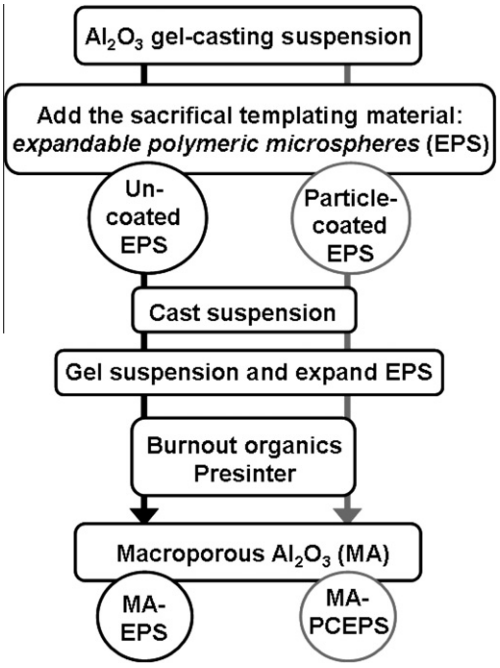

Fig. 1. Flow chart of the manufacturing process for the macroporous alumina materials.

the pores in the macroporous alumina materials. The EPS (ON316WUX, Expancel, Sweden) consist of a co-polymer shell and are filled with a blowing agent (isobutane). The mean particle size (D50) of the EPS used in this work is 33 μm in the unexpanded state.

We coated the EPS with a layer of alumina particles using a polyelectrolyte multilayer as a binder. The polyelectrolytes used in this study were: poly(ethyleneimine) (ammonium salt, 99% purity, $Mw = 10.000$) abbreviated PEI; poly(acrylic acid) (sodium salt, 25 wt.% in water, $Mw = 50.000$) abbreviated PAA; and poly(allylamine hydrochloride) ($Mw = 60.000$) abbreviated PAH. PAA and PAH were acquired from Polysciences Europe GmbH, Germany, and PEI from Polysciences Inc., USA. After each addition of polyelectrolyte at a concentration of 1 wt.% with respect to the EPS, the EPS dispersion (5 wt.% in 0.01 M NaCl (puriss p.a., Sigma–Aldrich, Sweden)) was stirred for 20 min, and excess polyelectrolyte was removed by filtering the EPS three times. This process was repeated using polyelectrolytes of different charge. The polyelectrolyte-covered surfaces of the EPS were coated with a layer of submicron-sized alumina particles (AKP-30, Sumitomo Chemical Co. Ltd, Japan). The EPS suspension was slowly added in four portions to a 1 wt.% alumina suspension at pH 5 during stirring. The mixture was stirred overnight. A final layer of polyelectrolyte was added onto the particle-coated EPS. The particle-coated EPS were slowly dried for several days at 30 °C in 10% relative humidity. All steps in the layer-by-layer coating procedure were performed at room temperature.

We produced the macroporous alumina by gel casting an alumina suspension containing a monomer and cross-linker together with the EPS that act as a template for

Please cite this article in press as: Andersson L et al. Permeability, pore connectivity and critical pore throat control of expandable polymeric sphere templated macroporous alumina. Acta Mater (2010), doi:10.1016/j.actamat.2010.10.056

the pores. The EPS were either uncoated or coated with alumina particles. The suspension was based on the alumina powder AKP-30 (Sumitomo Chemical Co. Ltd., Japan) with an average particle size (D50) of 0.31 μm. The alumina powder was dispersed in the suspension with the polyelectrolyte Darvan 821A (Vanderbilt Company Inc., USA). We used methacrylic acid (Sigma–Aldrich Sweden AB, Sweden) and N,N′-methylenebisacrylamide (Sigma–Aldrich Sweden AB, Sweden) as the monomer and cross-linker, respectively. Ammonium persulfate (APS) (Sigma–Aldrich Sweden AB, Sweden) was used as the initiator for the polymerization of the monomer and cross-linker. The polymeric spheres expanded in the mixture of EPS, alumina powders and monomers and cross-linkers in a similar temperature range as the monomer and cross-linker form a gel. The gel-casting process with EPS to produce macroporous ceramics is described in detail in previous work [19]. The organic materials were removed at 600 °C prior to pre-sintering the macroporous alumina at 1200 °C.

2.2. Characterization

The zeta potential was measured with a Zetasizer Nano ZS instrument (Malvern Instruments Inc., London, UK). The standard deviation was calculated from the five zeta potential measurements and represented as error bars on each point.

Thermo-mechanical analysis (TMA) of the particle-coated and uncoated EPS was performed with a Mettler Toledo TMA/SDTA841e with STARe software. The measurements were done in air at a heating rate of 20 °C min^{-1} and with a net load of 0.06 N.

The particle-coated EPS were imaged with a field emission scanning electron microscope (FE-SEM), JSM-7000F (JEOL, Japan) at an acceleration voltage of 2.5 kV. The macroporous alumina materials were studied with a Zeiss UltraPlus FE-SEM at an acceleration voltage of 20 kV.

The porosity and pore throat diameters of the porous alumina were evaluated by mercury intrusion porosimetry (Micromeritics AutoPore III 9410), assuming a surface tension and contact angle of mercury of 485 m N m^{-1} and 130°, respectively.

2.3. X-ray μ-CT

The X-ray μ-CT instrument was developed and built at the Australian National University [21]. The instrument operates with a cone beam geometry with a spot size of 2 μm. Cylinders with a diameter of 5 mm were extracted from the middle of macroporous alumina blocks and imaged with the X-ray source operating at 80 kV and with a beam current of 100 μA. The 2048^3 voxel tomograms consist of a set of 2880 two-dimensional (2D) radiograph projections that were acquired at different rotation angles covering the complete 360°. A 1 mm thick dense aluminum filter was placed in front of the alumina cylinder to reduce the problem of beam hardening of the polychromatic beam, which may lead to artifacts in the radiographs [21]. The resulting voxel dimension was 3 μm.

The 2D radiographs were first pre-processed to minimize artifacts and then reconstructed with a Feldkamp algorithm to generate a tomogram consisting of voxels [21,22]. After reconstruction, the tomogram data, which are presented in gray levels corresponding to the density and composition of the alumina material, were treated with image enhancing filters to reduce noise and blur [23,24]. A segmentation method known as *converging active contours* [24] was used to categorize the 3D data as either solid or void. Simple thresholding is not sufficient to capture thin phase boundaries at the instrument resolution limit in these irregularly shaped porous bodies with thin walls and a wide pore size distribution [24].

The total porosity of the macroporous materials was derived from the segmented X-ray μ-CT data by normalizing the number of voxels of the pore phase by the total number of voxels. The pores are connected into clusters that could be identified and labelled using a burning algorithm across the voxel faces, ignoring connections across corners or edges [25]. The clusters that are isolated and disconnected from the largest cluster could thus be distinguished.

In the next step of the 3D analysis, the pores and the pore throats were identified using an algorithm based on a Euclidean distance map of the segmented data, which associates to each pore voxel the nearest distance to a solid phase voxel [26]. A watershed function applied to this distance map partitioned the pore space into pore bodies. The watershed transform expands from a seed voxel situated at each pore center to identify each individual pore space [26,27]. The pore network was generated using a refined medial axis transform [26,28,29]. This method preserves the topology of the network, without creating loops or excess merging of pores. A maximum covering sphere algorithm was applied to calculate the pore throat diameter at the smallest constriction of each throat.

All image processing steps were performed with the software Mango 3D Parallel Image Analysis Toolkit [26], and the 3D data volumes were visualized with the volume exploration program Drishti [30].

2.4. Permeability

The permeability was calculated using a lattice-Boltzmann (LB) method [31]. The LB approach is a mesoscopic numerical method used in computational fluid dynamics, where the macroscopic dynamics of the solution of a discretized Boltzmann equation match the Navier–Stokes equation. Due to its simplicity in form and adaptability to complex flow geometries, like the presence of solid–fluid boundaries, one of the most successful applications of the LB method has been to simulate flow in complex porous media [31,32]. For computational reasons, the simulations were conducted on independent sub-domains from each

Please cite this article in press as: Andersson L et al. Permeability, pore connectivity and critical pore throat control of expandable polymeric sphere templated macroporous alumina. Acta Mater (2010), doi:10.1016/j.actamat.2010.10.056

macroporous alumina dataset with sizes between 724^3 and 1440^3 μm^3. The sub-volumes have dimensions six times larger than the mean pore size, which has been shown to be sufficient for accurate estimations of the permeability [33,34].

The permeability of each sub-volume was calculated by applying a small pressure gradient to the liquid in one direction [32]. For computational simplicity, the outer boundaries of the sub-volume parallel to the pressure gradient were modeled according to the mirror-image boundary condition, and the outer boundaries perpendicular to the pressure gradient were saturated by a thin layer of liquid. In the direction of flow, the liquid medium was made quasi-periodic; any liquid exiting the porous body re-entered at the opposite face [33]. We also assume the no-slip boundary condition at solid–fluid interfaces [31]. The presented permeability values are the restriction of the permeability tensor to the direction of the pressure gradient.

2.5. Calculation of tortuosity and critical pore radius

The tortuosity of the porous phase was determined by modeling the voxelated material as a network of electrical resistors and determining the electrical conductivity across the 3D dataset [34]. The voxels were converted into an electrical network by modeling each pair of adjacent voxels as being nodes connected by a resistor. The resistors in the solid phase were assigned the conductivity $\sigma_{solid} = 0$ while those in the pore phase, i.e. saturated with fluid, were assigned a normalized conductivity: $\sigma_{fluid} = 1$. A potential gradient was applied across the volume and the system was relaxed using a conjugate gradient technique to evaluate the field to solve the Laplace equation with charge conservation boundary conditions. The tortuosity is given by the ratio between the effective resistance to electrical current flow across the fluid saturated pore phase (σ_{eff}) divided by the conductance of the fluid (σ_f) and the porosity (ϕ) [34]:

$$\frac{\sigma_{eff}}{\sigma_f} = \frac{\phi}{\tau} \quad (1)$$

The critical pore diameter l_c is a length-scale that relates to the size of the largest sphere which can percolate across a connected pore system [20]. We derived l_c from the inflection point in simulated mercury capillary pressure curves for each sub-volume. The pressure curve is calculated by simulating the intrusion of spheres with incrementally smaller radius until the pore phase is completely invaded. For the simulation we used a surface tension of $\gamma_{air-Hg} = 485$ m N m^{-1} and we assumed that all outer faces of the sub-volume were in contact with the simulated mercury.

3. Results and discussion

3.1. Particle coating of expandable polymeric spheres

We modified the surfaces of the expandable polymeric spheres (EPS) by sequential adsorption of charged species (anionic and cationic polyelectrolytes and colloidal alumina) using layer-by-layer adsorption. An adsorbed layer of alumina particles on the EPS is desirable to form an effective boundary layer of particles around the EPS in the gel-casting suspension. The layer-by-layer adsorption was performed in a neutral pH range, where the weak polyelectrolytes are highly dissociated. Fig. 2 shows that the cationic polyelectrolyte poly(ethyleneimine), abbreviated PEI, which is well known to adsorb strongly [35], resulted in a significant positive charge on the EPS.

Several layers of the anionic poly(acrylic acid), abbreviated PAA, and the cationic poly(allylamine hydrochloride), abbreviated PAH, were sequentially added onto the PEI-coated EPS. Fig. 2 shows that the sign of the zeta potential changed with each addition; the addition of PAA produced a negative surface charge and the addition of PAH produced a positive surface charge. The switch in the sign of the surface charge is characteristic for the layer-by-layer process and shows that the most recently adsorbed polyelectrolyte dominates the surface charge [36]. Positively charged alumina particles (at pH 5) were adsorbed onto the EPS surfaces that had been coated with four polyelectrolyte layers, having an outermost PAA coating with a strongly negative surface charge (Fig. 2). The layer-by-layer coating was finished off with a final layer of PAA adsorbed onto the alumina particles to increase the compatibility of the coated EPS with the concentrated alumina suspension containing monomers and cross-linkers in solution.

The SEM images in Fig. 3a and b show that the alumina particles formed a dense layer on the surface of the EPS. The energy dispersive X-ray spectroscopy (EDS) line scan shows a high intensity of the Al (Ka) and O (Ka) signals over the expandable polymeric sphere surface compared

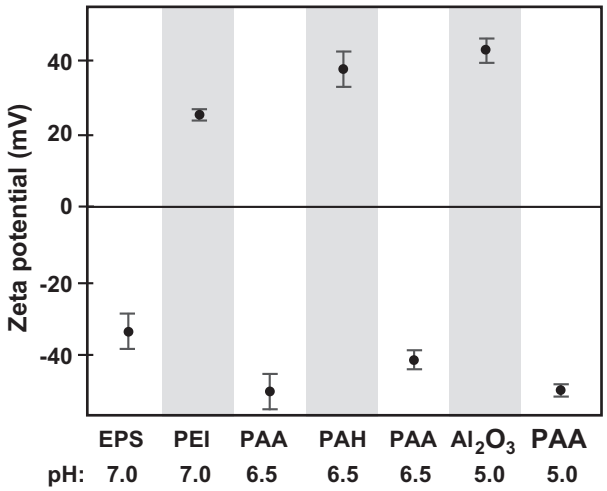

Fig. 2. The zeta potential of the EPS after sequential adsorption of polyelectrolytes and alumina (Al_2O_3) particles. The polyelectrolytes used were poly(ethylene imine) (PEI), poly(allylamine hydrochloride) (PAH) and poly(acrylic acid) (PAA). The mean value and the standard deviation of the zeta potential are indicated for each polyelectrolyte addition, together with the pH value for the adsorption.

Please cite this article in press as: Andersson L et al. Permeability, pore connectivity and critical pore throat control of expandable polymeric sphere templated macroporous alumina. Acta Mater (2010), doi:10.1016/j.actamat.2010.10.056

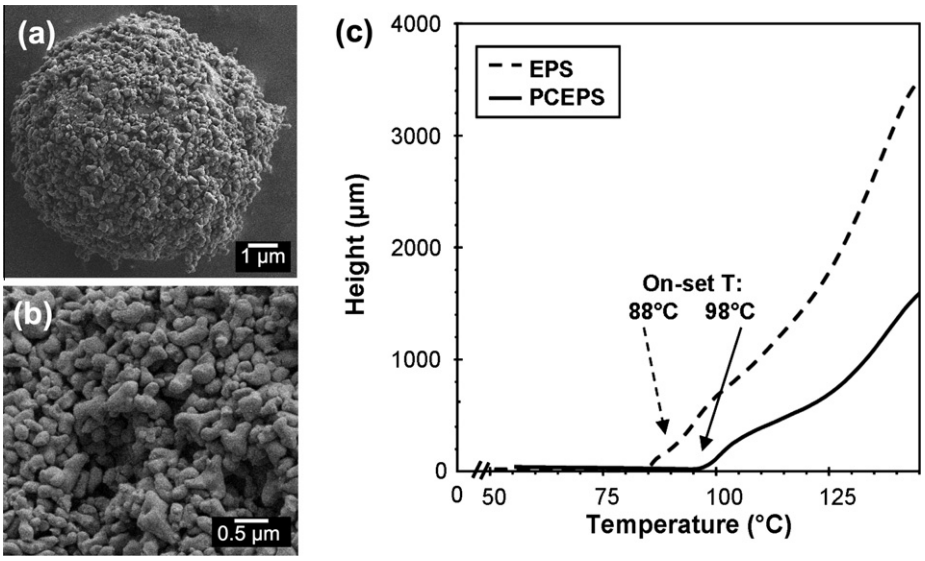

Fig. 3. The sacrificial templates, the EPS, were coated with a layer of alumina particles. Scanning electron microscopy images of (a) an alumina particle-coated EPS (PCEPS), (b) a close-up of the surface morphology of the PCEPS, and (c) shows thermo-mechanical analysis on the uncoated EPS and PCEPS for the on-set temperature of expansion.

to the signals from the silica-substrate background (see the Supplementary data (SD) section, Fig. S1).

The EPS are filled with a blowing agent that expands when heated. Thermo-mechanical analysis on the uncoated and particle-coated EPS (PCEPS) showed that the particle coating acted as a crust around the spheres and shifted the temperature-induced expansion of the EPS from 88 °C to 98 °C (Fig. 3c). The particle-coated EPS had also expanded less than the uncoated EPS when the expansion was complete.

3.2. Sacrificial templating with expandable polymeric spheres and characteristics of the macroporous materials

The macroporous alumina materials were produced by gel casting a suspension of alumina with a monomer and cross-linker together with EPS. The EPS, both uncoated and particle-coated (PC), acted as a templating material for the macropores. The gel-casting suspension was cast into cylindrical moulds, which restricted the expansion of the EPS in the (horizontal) *xy*-plane, but left them free to expand in the (vertical) *z*-direction. The monomer and cross-linker, which gelled upon heating to 80 °C, preserved the porous structure created by the EPS before burnout and pre-sintering. Table 1 shows how the porosity of the macroporous alumina materials, as determined by X-ray μ-CT, varied with the amount of added EPS. As a result of the alumina particle layer, which restricted the expansion of the spheres, it was necessary to add a higher amount of particle-coated EPS compared to the amount of uncoated EPS to reach similar porosity levels in the macroporous alumina materials. This production process, based on the simultaneous expansion of the polymeric spheres and gelling of the monomer and cross-linker, has been described in detail in previous work [19].

Table 1
Porosity derived with X-ray μ-CT of macroporous alumina materials templated with uncoated expandable polymeric spheres (EPS) or alumina particle-coated EPS (PCEPS).

Material label[a]	Expandable polymeric spheres (wt.% dwb)[b]	Porosity (vol.%)
MA-EPS-76	1.8	76
MA-EPS-57	1.1	57
MA-EPS-51	0.7	51
MA-EPS-46	0.3	46
MA-PCEPS-67	4.5	67
MA-PCEPS-48	2.4	48

[a] The number at the end of each material label refers to the level of porosity in the material as determined by X-ray μ-CT.
[b] The amount of sacrificial templating material, without alumina particle coating, in the gel-casting suspension in wt.% dry weight basis (dwb).

Fig. 4 shows SEM images of MA-PCEPS-48 and MA-EPS-51 parallel to the corresponding 2D slices from the X-ray CT data, respectively. We identified these specific 2D slices from the *xy*-plane of the tomogram and segmented data by applying an aligning algorithm to the 3D dataset [37]. The images of the macroporous alumina (MA) in Fig. 4 show the difference in pore sizes in the *xy*-plane between materials templated with uncoated EPS (MA-EPS-51) and particle-coated EPS (MA-PCEPS-48). As a result of the alumina particle layer, which restricted the expansion of the particle-coated spheres, MA-PCEPS-48 showed a higher number of pores with smaller pore sizes compared to MA-EPS-51.

The X-ray μ-CT data in Fig. 5b and d show that particle-coated EPS created a narrower pore size distribution compared to uncoated EPS in macroporous alumina materials.

Please cite this article in press as: Andersson L et al. Permeability, pore connectivity and critical pore throat control of expandable polymeric sphere templated macroporous alumina. Acta Mater (2010), doi:10.1016/j.actamat.2010.10.056

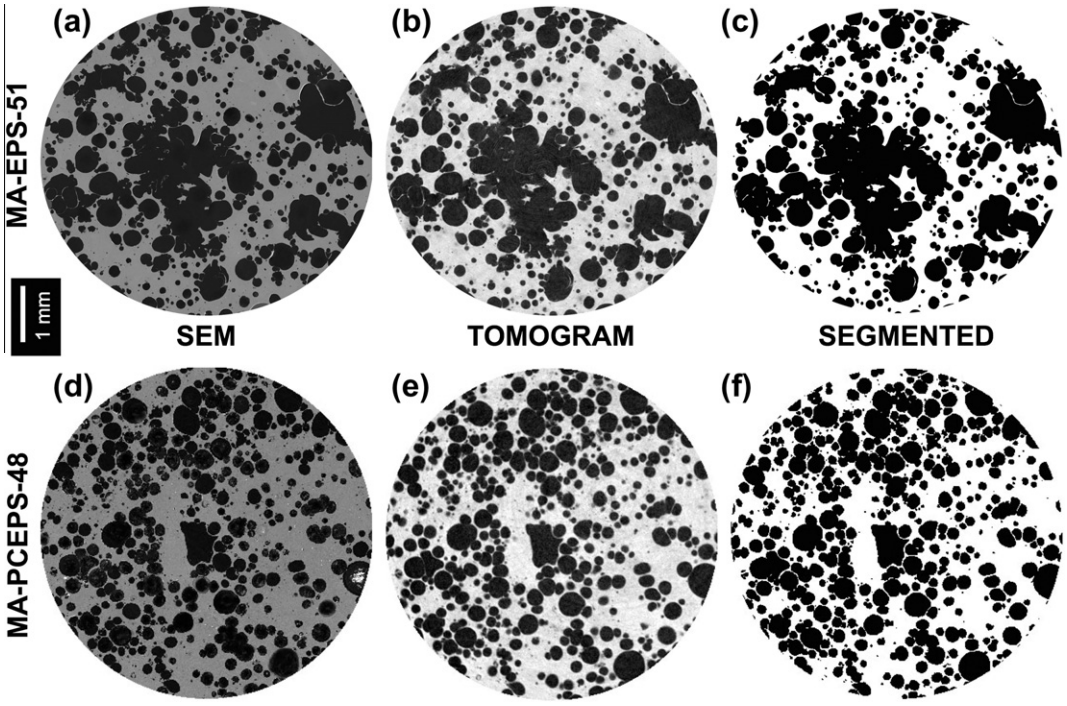

Fig. 4. SEM images and corresponding two-dimensional slices retrieved from the three-dimensional X-ray micro-computed tomography data for macroporous alumina. The SEM images (a and d) are compared with gray-scale tomogram data (b and e) and with segmented representations (c and f) with the pores in black and the solid in white. The macroporous alumina materials MA-EPS-51 and MA-PCEPS-48 were templated with uncoated and particle-coated expandable polymeric spheres (EPS and PCEPS), respectively.

Templating with PCEPS resulted in an increase in the fraction of isolated pore clusters compared to templating with EPS (Fig. 6). The particle coating on the EPS not only reduced the expansion of the EPS but also introduced a barrier of alumina particles to separate the pores in the pre-sintered alumina. Fig. 6 also shows that the fraction of isolated clusters decreased as a function of increasing total porosity for all the macroporous alumina materials.

The mercury porosimetry data in Fig. 7 quantifies the size of the smallest pore diameter, i.e. the cell windows or throats, over several orders of magnitude. The throats below 1 μm in size are due to interstices between alumina particles, while the larger throats of size 1–300 μm are caused by the sacrificial templating material.

The particle-coated EPS resulted in relatively small throats, up to 20 μm, in the low-porosity material MA-PCEPS-48 while the high-porosity material MA-PCEPS-67 displayed throats up to 240 μm. The uncoated EPS resulted in 30–300 μm sized throats in the low-porosity material MA-EPS-46 and 8–260 μm sized throats in the high-porosity material MA-EPS-76. The smaller throats for the MA-PCEPS compared to the MA-EPS suggest that the particle coating forms a crust around the spheres that reduces the coalescence of the EPS when they expand.

A third measure to indicate how well the pore phase is connected, apart from the fraction of isolated pore clusters and throat size distribution, is the number of pores that each pore is connected to. The distribution of the number of connected pore neighbors is plotted as their relative frequency of occurrence in Fig. 8. The distribution gets narrower with decreasing average porosity in the macroporous alumina. MA-PCEPS-48 stands out with a small and narrow distribution of the number of connected pore neighbors. (The distribution of the number of connected pore neighbors for MA-EPS-51 and MA-EPS-57 are shown in SD, Fig. S2.)

The connectivity of the pore phase for MA-PCEPS-48 is visualized in Fig. 9 by a pore-network model of this macroporous alumina material templated with particle-coated EPS. The actual pore volumes were not included for clarity. Fig. 9a shows that some regions of the pore volume are completely disconnected and that the pore volume does not percolate. The connectivity of the pore phase is highlighted in Fig. 9b, in which the isolated clusters that are not connected to the main percolating pore phase have been removed. (Pore-network models of other macroporous alumina materials are presented in SD, Fig. S3.) The pore-network model and the number of connected pore neighbors are derived from a medial axis algorithm applied to the 3D dataset [26].

3.3. Permeability

The differences in local flow paths of fluid permeating the macroporous alumina materials templated with uncoated EPS and particle-coated EPS are visualized three-dimensionally in Fig. 10. The two macroporous EPS and PCEPS-templated alumina materials in Fig. 10

Please cite this article in press as: Andersson L et al. Permeability, pore connectivity and critical pore throat control of expandable polymeric sphere templated macroporous alumina. Acta Mater (2010), doi:10.1016/j.actamat.2010.10.056

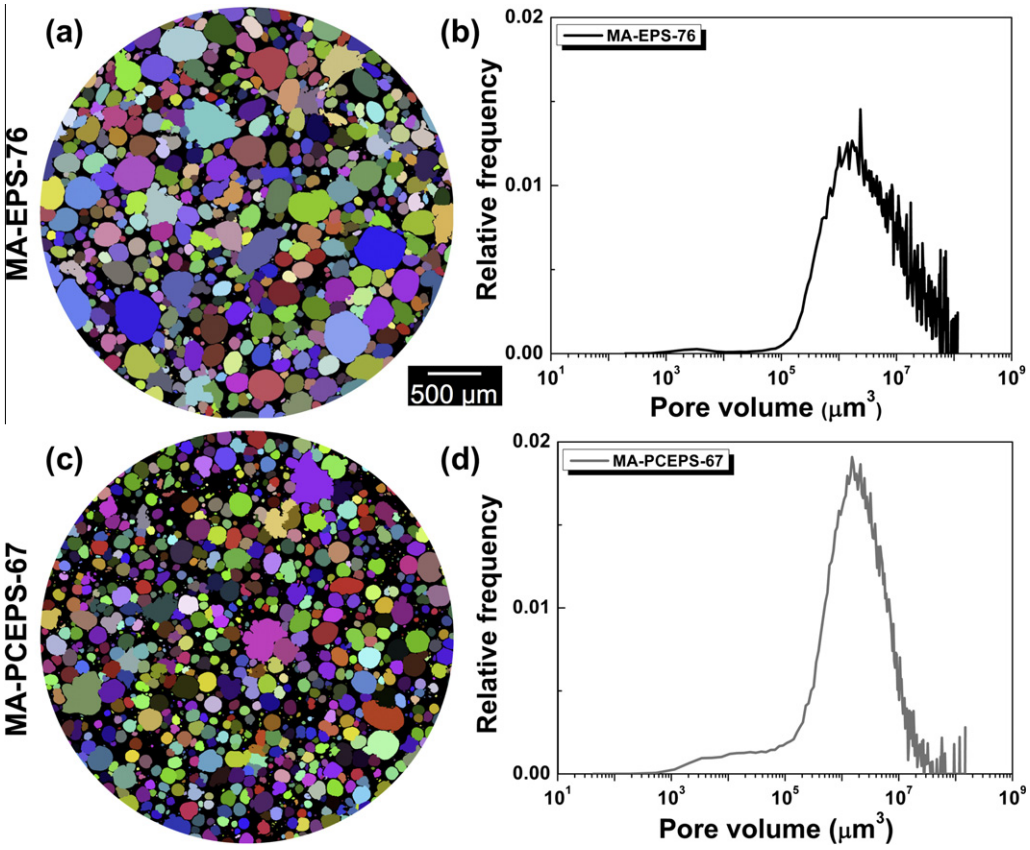

Fig. 5. The pore volume distribution (right) and representative two-dimensional slices (left), with each pore individually colored, from the X-ray micro-computed tomography data. The macroporous alumina material MA-EPS-76 in (a) and (b) was templated with uncoated expandable polymeric spheres (EPS), and MA-PCEPS-67 in (c) and (d) with alumina particle-coated EPS (PCEPS). (For interpretation of the references to color in this figure legend, the reader is referred to the web version of this article.)

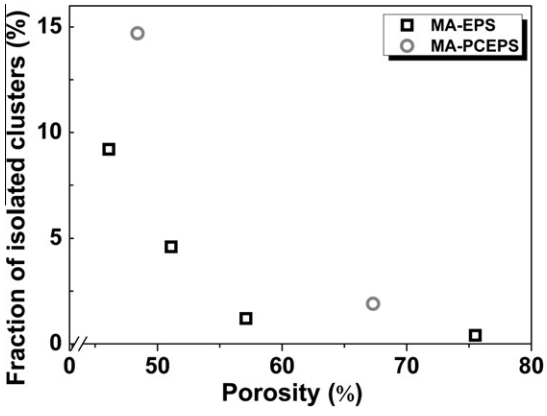

Fig. 6. The fraction of isolated pore clusters as a function of the total porosity (%) for macroporous alumina (MA). The materials were produced using uncoated or particle-coated (PC) expandable polymeric spheres (EPS) as sacrificial templates. The data was retrieved from the X-ray micro-computed tomography analysis.

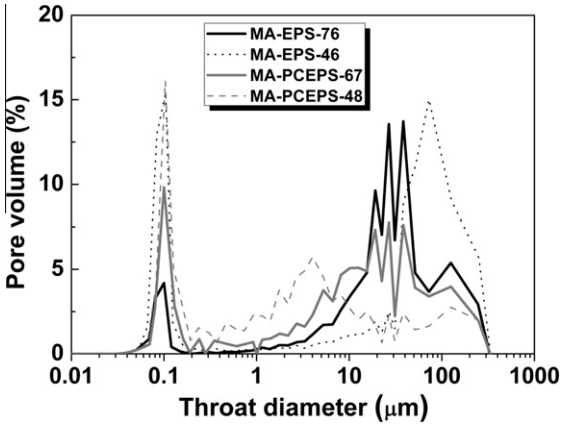

Fig. 7. Throat size distributions of macroporous alumina determined by mercury porosimetry. MA-EPS-76 and MA-EPS-46 were templated with uncoated expandable polymeric spheres (EPS) and MA-PCEPS-67 and MA-PCEPS-48 were templated with particle-coated EPS (PCEPS).

had similar porosities (46% and 48%, respectively) but quite different velocity and flow fields: in MA-EPS-46 (Fig. 10a) the fluid mainly permeated through wide passages, whereas in MA-PCEPS-48 (Fig. 10b) the fluid flow was constricted by narrow pathways between spherically shaped pores. The velocity fields represent the dominating flow in the x-direction and were derived from the calculated permeability. In the on-line version of this article, additional video data is available of the velocity intensities and local flow fields visualized in three-dimensions.

Please cite this article in press as: Andersson L et al. Permeability, pore connectivity and critical pore throat control of expandable polymeric sphere templated macroporous alumina. Acta Mater (2010), doi:10.1016/j.actamat.2010.10.056

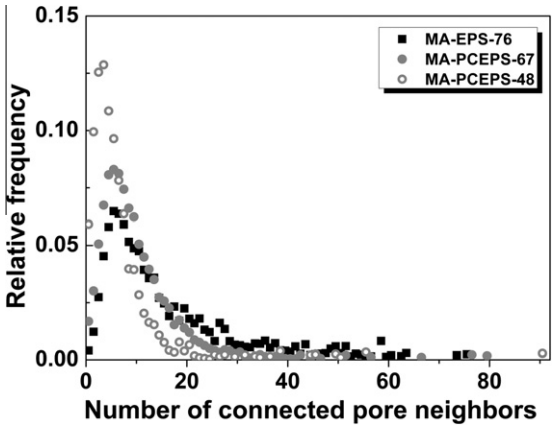

Fig. 8. The distribution of the number of connected pore neighbors is shown as its relative frequency of occurrence in macroporous alumina materials templated with uncoated expandable polymeric spheres (EPS) or particle-coated EPS (PCEPS). The porosities of the macroporous alumina materials were 76%, 67% and 48%, respectively.

Fig. 11 shows the permeability to fluid flow in the x- and z-directions calculated on sub-volumes from the sacrificially templated macroporous alumina. The difference in permeability in the two different directions is probably related to the features of the production process: the suspension was cast into cylindrical moulds which restricted the expansion in the xy-plane, but allowed expansion in the z-direction. Fig. 11 shows that the permeability of the macroporous alumina increased with increasing porosity. The permeability was lower for the materials templated with PCEPS compared to the materials templated with uncoated EPS.

The permeability, κ, of a porous material is commonly determined using Darcy's law:

$$Q = \frac{\kappa \cdot \Delta P}{\mu} \frac{A}{L} \tag{2}$$

where Q is the amount of transported liquid, ΔP the pressure drop, μ the viscosity, the area A is the cross-sectional area available for fluid flow and L is the length over which the pressure drop is measured.

The Katz–Thompson model,

$$\kappa = \frac{C \cdot \phi \cdot l_c^2}{\tau} \tag{3}$$

is a commonly used model that is derived from Darcy's law. The model requires information on the porosity (ϕ), the critical pore diameter (l_c), the tortuosity (τ) and a constant C, which depends on the distribution of pore sizes in the material. The critical pore diameter, which corresponds to the diameter of the smallest constriction of a set of pores that percolate through the porous structure, is in this study obtained from the inflection point of the simulated mercury intrusion curve [20].

The tortuosity of the porous paths is an important factor in the Katz–Thompson model. It is given by the ratio between the effective resistance (σ_{eff}) of electrical current across the pore phase filled with fluid to the conductance of the fluid itself (σ_f), which we calculated for each sub-volume and for every direction (x, y and z) [34].

Fig. 12 shows the permeability predicted by the Katz–Thompson model plotted against the simulated permeability for macroporous alumina templated with uncoated EPS and particle-coated EPS, respectively. The permeability was simulated in all directions (x, y and z) using sample volumes (1.44^3 mm^3) eight times larger than the volumes used for simulation in Fig. 11 to reduce the scatter. Although the value of the constant C in the Katz–Thompson model varies slowly over a wide range of pore shapes and pore size distributions [38] we used $C = 0.04$ in correspondence with previous studies [33,34]. We found that values calculated with the Katz–Thompson model were in good agreement with the simulated permeability over the

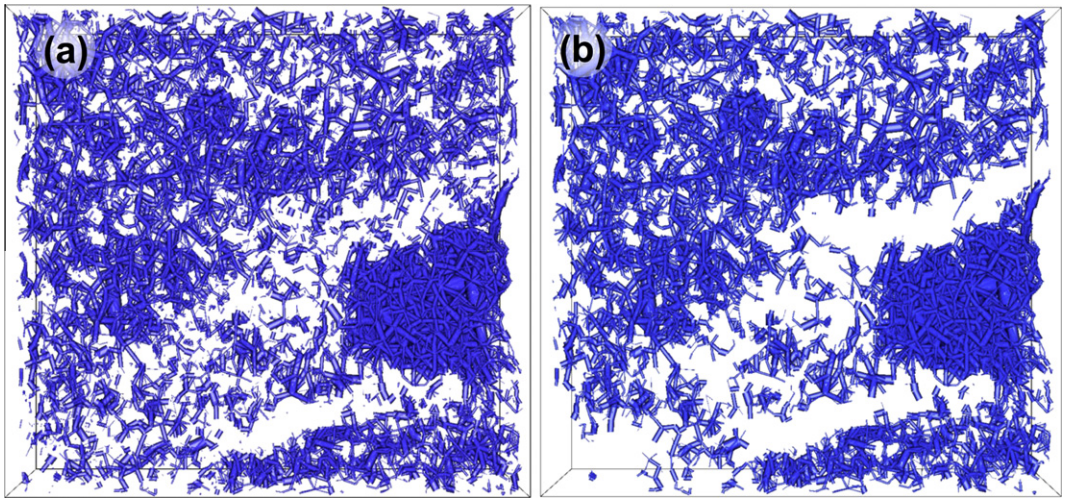

Fig. 9. Pore-network models of a macroporous alumina material templated with particle-coated (PC) expandable polymeric spheres (EPS) (MA-PCEPS-48). The isolated clusters of pores that are separated from the main pore phase remain in (a) but have been removed in (b). The connections between pores are represented by cylinders between pore centres. These pore-network sections measure $5.3 \times 0.6 \times 5.0$ mm^3.

Please cite this article in press as: Andersson L et al. Permeability, pore connectivity and critical pore throat control of expandable polymeric sphere templated macroporous alumina. Acta Mater (2010), doi:10.1016/j.actamat.2010.10.056

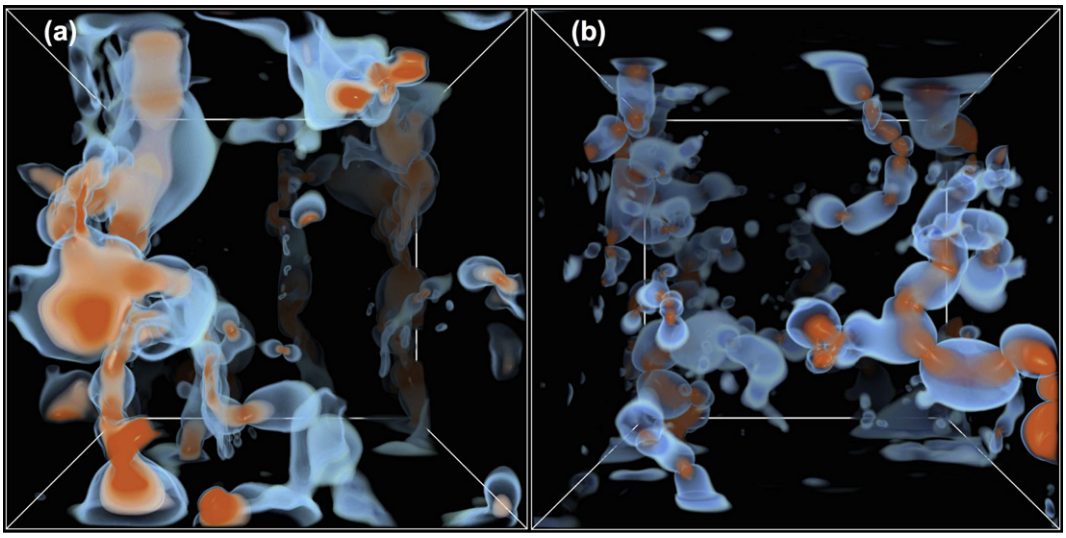

Fig. 10. Three-dimensional visualizations showing snapshots of the velocity intensities and local flow paths in macroporous alumina materials. The flow paths, advancing in the vertical direction, were derived from simulations of permeability. The darker color (red) represents a high flow velocity. The volumes correspond to 1.44^3 mm^3 of macroporous alumina materials templated with uncoated expandable polymeric spheres (EPS) or particle-coated EPS (PCEPS): MA-EPS-46 in (a) and MA-PCEPS-48 (b). (For interpretation of the references to color in this figure legend, the reader is referred to the web version of this article.)

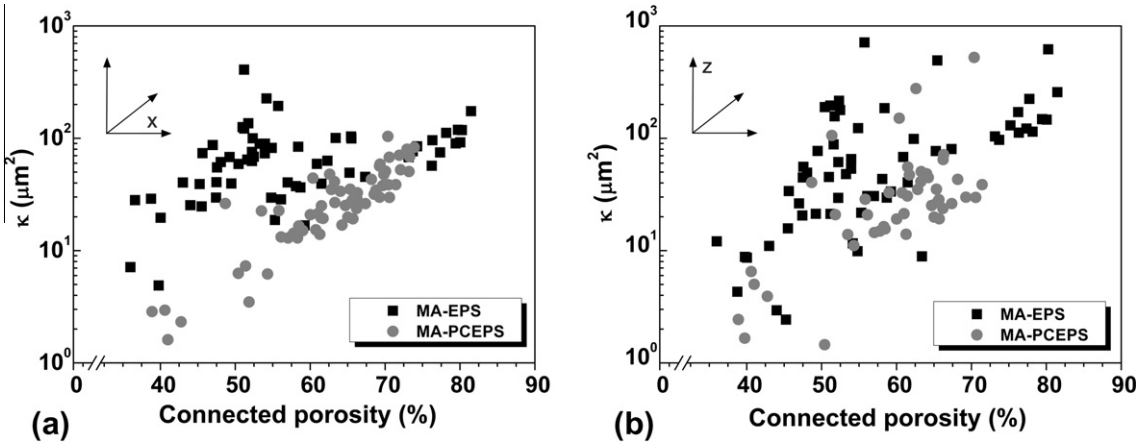

Fig. 11. Simulated permeability plotted as a function of connected porosity for sub-volumes of macroporous alumina templated with uncoated expandable polymeric spheres (EPS) or particle-coated EPS (PCEPS).

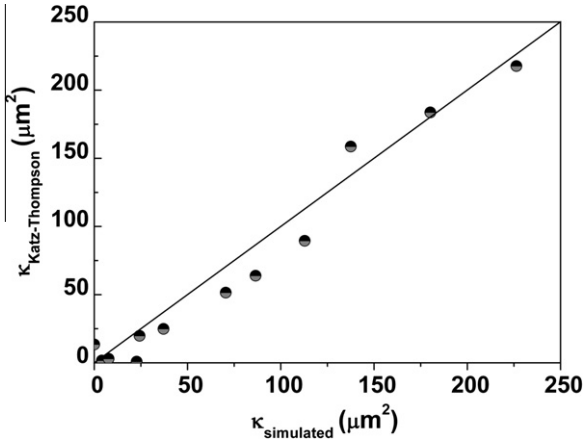

Fig. 12. Comparison of the simulated permeability to the estimated permeability derived with the Katz–Thompson model for macroporous alumina templated with uncoated expandable polymeric spheres (EPS) and particle-coated EPS (PCEPS), respectively.

investigated permeability range. This agreement indeed suggests that it is the smallest constrictions in an assemblage of connected pores that govern the fluid flow through the macroporous alumina materials.

4. Conclusions

The connectivity and the size of pore throats (windows) in macroporous alumina have been tuned by a modified sacrificial templating method. We coated the templating material, expandable polymeric spheres (EPS), with ~10 wt.% (dry weight basis) alumina particles using layer-by-layer adsorption of polyelectrolytes and alumina particles. We then incorporated the coated EPS in a gel-casting suspension, induced an expansion of the spheres, removed the organic template, and pre-sintered the alumina materials.

Please cite this article in press as: Andersson L et al. Permeability, pore connectivity and critical pore throat control of expandable polymeric sphere templated macroporous alumina. Acta Mater (2010), doi:10.1016/j.actamat.2010.10.056

The particle coating on the EPS resisted the heat-induced expansion of the spheres and thus resulted in smaller pores and lower porosities compared to uncoated EPS. We have shown that the particle coating on the EPS reduced the coalescence of the expanding spheres, which doubled the fraction of pore clusters isolated from the main percolating pore phase when templating with particle-coated EPS vs. uncoated EPS. Three-dimensional analysis with X-ray μ-CT showed that the particle coating reduced the dimensions of the cell windows (throats) by two orders of magnitude. The particle coating also decreased the number of cell windows (connections) between neighboring pores.

We used a lattice-Boltzmann method to simulate the permeability to fluid flow in the macroporous alumina from the 3D data acquired by X-ray μ-CT. The permeability was decreased by up to two orders of magnitude when templating with particle-coated EPS compared to uncoated EPS in macroporous alumina materials of similar porosities. The simulated permeability and the permeability estimations from the Katz–Thompsons model were in good agreement over the whole range of investigated permeability for all macroporous alumina materials. This agreement suggests that the permeability in the macroporous alumina materials is governed by the critical pore throat diameter.

Acknowledgments

The Swedish Research Council (VR) and the Berzelii Center EXSELENT on porous materials are acknowledged for financial support. L. Andersson acknowledges the Swedish Chemical Society and Knut and Alice Wallenberg foundation for travel grants. The ANU Electron Microscopy Unit is thanked for the use of the Zeiss UltraPlus analytical FE-SEM. The Wallenberg Foundation is acknowledged for supporting the EM center at the Department of Material and Environmental Chemistry at Stockholm University. K. Jansson is acknowledged for support on the EDS measurements. We recognize B. Malzacher and the colleagues at the Department of Applied Mathematics and A. Limaye at the Vizlab at the ANU for assistance with the data analysis and for valuable discussions. T. Castle is acknowledged for language assistance. We thank J. Nordin at Expancel AB, Sweden, for kindly providing the expandable spheres and the related TMA and TG data.

Appendix A. Supplementary material

Supplementary data associated with this article can be found, in the online version, at doi:10.1016/j.actamat.2010.10.056.

References

[1] Twigg MV, Richardson JT. Chem Eng Res Des 2002;80:183.
[2] Scheffler F, Claus P, Schimpf S, Lucas M, Scheffler M. Heterogeneously catalyzed processes with cellular ceramic monoliths. In: Scheffler M, Colombo P, editors. Cellular ceramics: structure, manufacturing, properties and applications. Weinheim: WILEY-VCH; 2005.
[3] Adler J. Int J Appl Ceram Technol 2005;2:429.
[4] Montanaro L, Jorand Y, Fantozzi G, Negro A. J Eur Ceram Soc 1998;18:1339.
[5] Gauckler LJ, Waeber MM, Conti C, Jacob-Dulière M. Light Met 1985:1261.
[6] Hench LL. J Am Ceram Soc 1998;81:1705.
[7] Burg KJL, Porter S, Kellam JF. Biomaterials 2000;21:2347.
[8] Knackstedt MA, Arns CH, Saadatfar M, Senden TJ, Limaye A, Sakellariou A, et al. Proc Roy Soc A 2006;462:2833.
[9] Despois J, Mortensen A. Acta Mater 2005;53:1381.
[10] Zhang Q, Lee PD, Singh R, Wu G, Lindley TC. Acta Mater 2009;57:3003.
[11] Spanne P, Thovert JF, Jacquin CJ, Lindquist WB, Jones KW, Adler PM. Phys Rev Lett 1994;73:2001.
[12] Petrasch J, Meier F, Friess H, Steinfeld A. Int J Heat Fluid Flow 2008;29:315.
[13] Moreno-Atanasio R, Williams RA, Jia X. Particuology 2010;8:81.
[14] Studart AR, Gonzenbach UT, Tervoort E, Gauckler LJ. J Am Ceram Soc 2006;89:1771.
[15] Green DJ, Colombo P. MRS Bull 2003;28:296.
[16] Du Z, Bilbao-Montoya MP, Binks BP, Dickinson E, Ettelaie R, Murray BS. Langmuir 2003;19:3106.
[17] Tang F, Fudouzi H, Uchikoshi T, Sakka Y. J Eur Ceram Soc 2004;24:341.
[18] Kim Y, Jin Y, Chun Y, Song I, Kim H. Scripta Mater 2005;53:921.
[19] Andersson L, Bergström L. J Eur Ceram Soc 2008;28:2815.
[20] Katz AJ, Thompson AH. Phys Rev B 1986;34:8179.
[21] Sakellariou A, Sawkins TJ, Senden TJ, Limaye A. Physica A 2004:339152.
[22] Feldkamp LA, Davis LC, Kress JW. J Opt Soc Am A 1984;1:612.
[23] Sakellariou A, Arns CH, Sheppard AP, Sok RM, Averdunk H, Limaye A, et al. Mater Today 2007;10:44.
[24] Sheppard AP, Sok RM, Averdunk H. Physica A 2004;339:145.
[25] Sheppard AP, Sok RM. Proc SPIE 2004;5535:166.
[26] Sheppard AP, Sok RM, Averdunk H. Proc Int Conf Soc Core Anal 2005:1.
[27] Sheppard AP, Sok RM, Averdunk H, Robins VB, Ghous A. Proc Int Conf Soc Core Anal 2006:1.
[28] Lindquist WB, Lee SM, Coker DA, Jones JW, Spanne P. J Geophys Res 1996;101B:8297.
[29] Silin D, Patzek T. SPE Annu Tech Conf Exhib 2003:1.
[30] Limaye A. Poster presentation. Vis 2006, Baltimore.
[31] Martys NS, Chen H. Phys Rev E 1996;53:743.
[32] Ferréol B, Rothman DH. Transp Porous Media 1995;20:3.
[33] Arns CH, Knackstedt MA, Pinczewski WV, Martys NS. J Petrol Sci Eng 2004;45:41.
[34] Arns CH, Knackstedt MA, Pinczewski MV, Lindquist WB. Geophys Res Lett 2001;28:3361.
[35] Lowack K, Helm CA. Macromolecules 1998;31:823.
[36] Hoogeveen NG, Cohen Stuart MA, Fleer GJ, Bohmer MR. Langmuir 1996;12:3675.
[37] Latham SJ, Varslot TK, Sheppard AP. ANZIAM J 2008;50:C534.
[38] Arns CH, Knackstedt MA, Martys NS. Phys Rev E 2005;72:046304.